energy&fuels

pubs.acs.org/EF

Article

Conversion Mechanism of Organic Components during the Eucalyptus Biomass Pyrolysis Process Based on the Multispectral Association Method

Xiao Lin, Meirong Dong,* Wei Nie, Gangfu Rao, and Jidong Lu

Cite This: *Energy Fuels* 2024, 38, 7929−7940

Read Online

ACCESS | Metrics & More | Article Recommendations | Supporting Information

ABSTRACT: It is important to understand the transformation mechanism of the pyrolysis process, which is a crucial method for thermally utilizing solid fuels. In this work, multispectral association technology was employed to measure the pyrolysis process of biomass (eucalyptus) and investigate the spatiotemporal characteristics of its gas−solid products. We utilized tunable diode laser absorption spectroscopy (TDLAS) to quantitatively measure the gases produced during the pyrolysis process (CH_4, H_2O), which reflects the progress of the pyrolysis. Laser-induced breakdown spectroscopy (LIBS) was used to qualitatively measure characteristic elements such as C, C_2, and H in the gas phase, revealing the product conversion trends. In addition, Raman spectroscopy was used to provide information about the molecular structure and functional group changes in biomass pyrolysis char. The evolving pattern of the Raman spectrum revealed that biomass char exhibits high reactivity during the dehydration and devolatilization stage, with a swift detachment of the methyl functional group. TDLAS and LIBS measurements revealed that a substantial amount of methane was produced, accompanied by the initial release peaks of the C and C_2 spectrum. During the secondary cracking stage, the reactivity and the rate of functional group detachment of biomass char gradually diminished. Methane production is relatively low in this stage, and the second-release peaks in the C and C_2 spectra might be associated with other organic gases generated through tar cracking. In addition, through multispectral association measurements on the samples with varying moisture content, it was found that moisture would increase the reactivity and the rate of functional group detachment of the biomass char, resulting in an increase in methane yield. Moreover, the spatial distribution characteristics of TDLAS and LIBS above the samples revealed that moisture facilitates the cracking of tar, resulting in the production of small molecular gases.

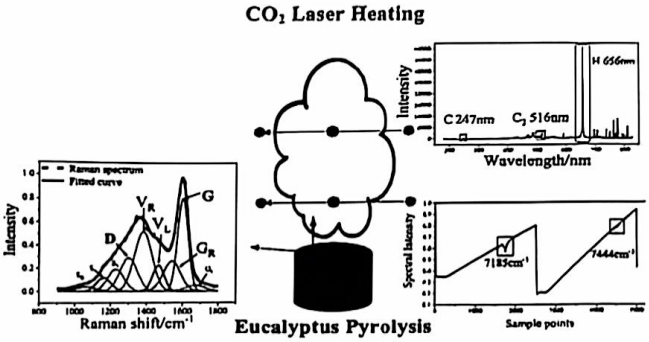

1. INTRODUCTION

Biomass, derived from living organisms including wood, crops, and aquatic plants, is a renewable and environmentally friendly source of energy.[1] Pyrolysis is an important method for the efficient thermal utilization of biomass. When biomass is heated in an inert atmosphere, it undergoes thermal decomposition and condensation reactions, transforming to solid biomass char, liquid bio-oil, and gaseous combustible gases. This process involves numerous products and reaction pathways.[2−5] Different types of biomass exhibit variations in the elemental composition and functional groups, which would result in variations in the pyrolysis products and their distribution of biomass. The eucalyptus belongs to the category of woody biomass, which is primarily composed of carbon, hydrogen, and oxygen elements. It contains various functional groups, including hydroxyl, carboxyl, aldehyde, and ketone groups, which can participate in reactions such as hydrolysis and condensation during the pyrolysis process. It is crucial to understanding the release patterns of important products and reaction processes during biomass pyrolysis, which can provide a foundational data set for investigating the mechanisms involved in biomass pyrolysis.

Traditional pyrolysis studies typically utilize heating equipment such as thermogravimetric analyzer (TGA), tube furnaces, and drop tube reactors to heat biomass, coupled with devices like Fourier transform infrared analysis (FTIR), gas chromatography (GC), and mass spectrometry (MS) to analyze the pyrolysis gas phase products under different conditions.[6−9] Yan et al.[10] and Huang et al.[11] used TGA-FTIR to detect the pyrolysis gas products of different biomass, simultaneously detecting gases such as CO, CO_2, CH_4, H_2O, NH_3, and HCN. Trubetskaya et al.[12] and Montiano et al.[13] characterized the tar produced from the pyrolysis of different

Received: January 10, 2024
Revised: March 22, 2024
Accepted: March 29, 2024
Published: April 9, 2024

https://doi.org/10.1021/acs.energyfuels.4c00154
Energy Fuels 2024, 38, 7929−7940

Table 1. Proximate Analysis and Ultimate Analysis of Biomass Samples[a]

	proximate analysis/%				ultimate analysis/%			
biomass sample	VM	FC	M	A	C	H	N	O
received basis	72.67%	15.91%	9.03%	2.39%	44.61%	5.56%	0.19%	49.5%
dry basis	79.88%	17.49%		2.63%	49.03%	5.01%	0.21%	45.53%

[a]VM is for volatile matter, FC is for fixed carbon, M is for moisture and A is for ash.

types of biomass at various heating temperatures using gas chromatography-flame ionization detection and mass spectrometry (GC-FID-MS). The solid phase char produced after biomass pyrolysis can be analyzed by Raman spectroscopy. Li et al.[14] and Keown et al.[15] utilized FT-Raman spectroscopy to investigate the structure of char in brown coal and sugar cane, respectively, fitting the spectra in the range of 800−1800 cm^{-1} and obtaining ten bands representing the major structures in char. Surup et al.[16] utilized various surface characterization techniques, including Raman spectroscopy, to analyze the influence of heating temperature on the carbon structure as well as other surface properties of char.

The traditional heating and gas analysis methods are suitable for describing the macroscopic thermal transformation process and revealing the release pattern of the final products.[17] However, offline analysis cannot directly capture the release processes of the components in the thermal conversion of fuels. This information is precisely the data most needed to establish biomass pyrolysis mechanisms and modeling.

The noncontact optical measurement methods allow for uninterrupted observation of intermediate transformation processes while remaining immune to the influence of flow fields and temperature in complex environments. Laser spectroscopy, including tunable diode laser absorption spectroscopy (TDLAS), and laser-induced breakdown spectroscopy (LIBS), is an optical method that obtains comprehensive in situ information on the temperature and concentration of components through laser interaction. It has been extensively used in the combustion field to reveal the thermal conversion mechanism.

TDLAS utilizes the absorption characteristics of the laser beam to quantitatively measure the concentrations of gas molecules. It has been used to monitor the intermediate conversion processes of specific gas components in complex reaction flow fields. In the application of TDLAS, Sepman et al.[18] utilized it to in situ measure CH_4, H_2O, soot, and gas temperature in the reactor core of a biomass gasifier, and found that CH_4 mainly originates from the pyrolysis of fuel particles in the lower temperature region of the reactor core, based on the spatiotemporal characteristics of CH_4. Furthermore, they measured the concentrations of H_2O, CO, and CO_2 during the combustion processes of diesel and biomass by TDLAS, and analyzed the composition of the exhaust gases by FTIR,[19] observing that diesel combustion was completed at the TDLAS measurement location, while wood combustion was still in progress. Qi et al.[20] used TDLAS for simultaneous measurements of soot volume fraction, H_2O concentration, and its temperature in an ethylene/air-premixed flame and obtained the distribution pattern of these components along the vertical direction of the combustor.

LIBS is an atomic emission spectroscopy technique capable of rapidly and simultaneously monitoring multiple elements, and it has been extensively employed for characterizing the temporal and spatial patterns of elemental changes within the combustion field. Wu et al.[21] utilized this technique to investigate the spatial characteristics of the C/H ratio in an ethylene-air premixed flame, directly observing the preferential diffusion of hydrogen relative to carbon. He et al.[22] applied LIBS for quantitative measurements of the release of alkali metals sodium and potassium during coal particle combustion. Li et al.[23] employed LIBS to measure relevant atomic and functional groups during the combustion of individual coal particles in different atmospheres, establishing a correlation between CN groups and the formation of NO_x. Kotzagianni et al.[24] used LIBS to analyze turbulent methane flames and found a linear relationship between H/O and C_2/CN spectral intensities with flame equivalence ratio. Furthermore, they used LIBS to identify and demarcate the flame structure and fuel distribution of hydrocarbon-air premixed laminar flames.[25]

Different optical measurement methods have their own characteristics in terms of application scenes and the scope of application. In recent years, researchers have made significant progress in the integration of multispectral technologies. Lee et al.[26] measured the H and O elements by LIBS and calculated the temperature by the H_2O absorption spectrum measured by the TDLAS, and realized the accurate inversion of the temperature and component concentration in the combustion field. Weng et al.[27] used LIBS and TDLAS to measure the atomic potassium concentration and total elemental potassium concentration of the burning biomass pallets. Deguchi et al.[28] used LIBS for online monitoring of trace elements and TDLAS for real-time measurement of O_2 and CO_2 concentrations in the incinerator. The combined use of various in situ spectroscopy techniques will achieve a synergistic diagnosis of the combustion field at both atomic and molecular dimensions.

To obtain more in situ information about the pyrolysis process, multispectral in situ techniques (LIBS and TDLAS) were applied to the measurement of gas−solid products in the pyrolysis process of biomass eucalyptus. TDLAS was utilized to quantitatively measure the concentrations of water vapors and methane of the gas phase products, while LIBS was utilized to qualitatively measure the characteristics of the elements in the gas phase products of pyrolysis, such as C, C_2, and H. The surface char molecular structure of biomass was characterized by Raman spectroscopy, which is combined with in situ optical measurements to reveal the mechanisms of gas−solid product conversion during biomass pyrolysis. Additionally, the spectral characteristics of biomass samples with received and dry basis were compared to clarify the influence of moisture on the pyrolysis process. The analysis of multiple spectral results allows for a comprehensive description of the spatial and temporal characteristics of pyrolysis gas−solid products, which contributes to a profound understanding of the complexity of biomass pyrolysis processes.

https://doi.org/10.1021/acs.energyfuels.4c00154
Energy Fuels 2024, 38, 7929−7940

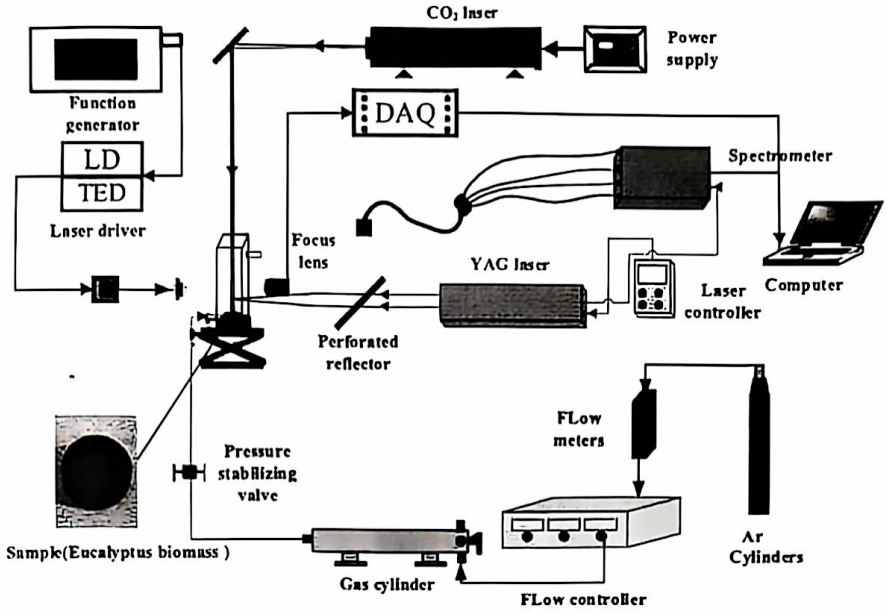

Figure 1. Experimental setup (a) LIBS measurement system; (b) TDLAS measurement system; (c) gas control system.

2. EXPERIMENTAL SETUP AND MEASUREMENT METHODS

2.1. Samples. Eucalyptus, as a valuable biomass resource, is characterized by rapid growth, high yield, and strong adaptability, which makes it a significant source of biomass energy.

Table 1 shows the proximate and ultimate analyses of eucalyptus powder, which was selected as the biomass fuel for this experiment.

To reduce the uncertainty of the experiments, the samples underwent identical preprocessing steps, including grinding, sieving, and uniform baking. Prior to the experiment, the eucalyptus biomass was ground into powder form and subsequently sieved through a sieve with one hundred mesh. This allowed for the selection of samples with a uniform particle size and controlled the moisture content of the samples. The biomass powder was pressed by using a mold to form a cylindrical single pellet solid fuel with a diameter of 6 mm and height of about 2.6 mm.

2.2. Experimental System and Methodology. CO_2 laser was used as a heat source for the pyrolysis of eucalyptus fuels, which is a kind of noncontact heating method, that is not affected by the measurement environment.[29,30] The experimental system consists of a reaction chamber, gas supply system, laser heating system, LIBS measurement system, and TDLAS measurement system, as shown in Figure 1.

The samples were placed in quartz tubes with a rectangular cross-section of 30 × 30 mm, which were placed on a height-adjustable displacement platform for easy adjustment of the measured positions. The sample was uniformly heated by a CO_2 laser with 60 W. Compared to traditional heating methods, CO_2 laser heating has several advantages. First, it efficiently converts laser energy into heat, enhancing energy conversion efficiency. Second, CO_2 laser heating provides high precision, allowing for precise heating of the surface of the samples and avoiding issues of overheating or uneven heating often associated with traditional methods. Additionally, as a noncontact heating method, CO_2 laser heating eliminates the need for direct contact with the heated object, mitigating the potential influences of the heating apparatus on spectral measurements. Last but not least, CO_2 laser heating exhibits a rapid response, allowing for quick adjustments in heating through modulation of laser power. Throughout the process, argon gas was continuously introduced into the reaction chamber at a rate of 3 L/min, ensuring rapid pyrolysis of the biomass in an inert atmosphere.

The LIBS measurement system employs a laser with a 1064 nm wavelength, which is focused on the gas product by a 50 mm focal length lens. The plasma radiation signal generated by the laser-induced breakdown of air is transmitted via an optical fiber to a four-channel spectrometer. The spectrometer detects wavelengths in the range of 180−815 nm, with a delay of 1.28 μs and an integration time of 1.05 ms. The system utilizes synchronous triggering of the spectrometer and YAG laser using a DG535.

The TDLAS system consists mainly of a function generator, laser controller, DFB laser, detector, and data acquisition module. It is used for the quantitative measurement of gas products CH_4 and H_2O during the biomass pyrolysis process using a two-line method for temperature detection. In the experimental process, a sawtooth wave current is generated by the function generator to make the DFB laser output continuous laser with a specific central wavelength.[31,32] The laser, passing through the pyrolysis chamber, is received by the detector, which obtains the laser attenuation signal. The detector signal is collected by the data acquisition module after passing through the transmission module. DFB lasers with central wavelengths of 1343 and 1392 nm are used to measure water vapor concentrations in the pyrolysis chamber, and temperature is measured by the two-line method. A DFB laser with a central wavelength of 1654 nm is used to detect the concentration of methane gas released during pyrolysis.

By adjusting the height of the displacement platform, the spatial and temporal characteristics of the gas phase products and their characteristic elements at heights of 1 and 10 mm above the biomass samples can be measured by LIBS and TDLAS. The unstable pyrolysis products released from the surface of the sample are measured at 1 mm, and the stable final products are measured at 10 mm; thus, we can analyze the variation pattern of the pyrolysis products in the gas phase space. In addition, biomass char samples were collected at different moments during the pyrolysis process, and their chemical structure was characterized by using the micro-Raman spectrometer (LabRAM Aramis) equipped with a 532 nm laser.

Furthermore, the generation of gas products during biomass pyrolysis is closely related to changes in the surface char structure. Therefore, Raman spectroscopy was utilized to characterize the surface carbon structure of biomass chars from different pyrolysis stages. By comparing the changes in surface activity and relevant functional group contents of biomass chars with the release patterns of pyrolysis product CH_4, the correlation between the solid phase and gas phase can be established, allowing a more comprehensive

https://doi.org/10.1021/acs.energyfuels.4c00154
Energy Fuels 2024, 38, 7929−7940

understanding of the organic transformation mechanisms during biomass pyrolysis. The experiments were repeated multiple times to reduce errors and mitigate the impact of fuel variations or measurement instability.

3. RESULTS AND DISCUSSION

3.1. Analysis of the Gas Phase Product Release Pattern by TDLAS. In this work, the specific DFB laser wavelength range used in the experiment allowed for the measurement of only CH_4 and H_2O molecules. Therefore, we divided the dehydration and devolatilization stage and the secondary cracking stage based on the release patterns of CH_4 and H_2O. TDLAS has the characteristic of a line of sight (LOS). The laser beam is emitted into the gas sample, and the transmitted signals are detected by the detector system. The gas sample is bound within the pyrolysis chamber, resulting in an effective optical path length of 30 mm, which corresponds to the diameter of the quartz tube. DFB lasers with center wavelengths of 1343 nm (7444 cm^{-1}) and 1392 nm (7185 cm^{-1}) were used to measure the concentration of water vapor released from the biomass particles as well as the temperature inside the pyrolysis chamber, and the DFB laser with center wavelength of 1654 nm (6046 cm^{-1}) was used to measure the concentration of methane released from the biomass particles. The concentrations of CH_4 and H_2O were calculated as averages along the optical path within the pyrolysis chamber, representing the average concentrations of CH_4 and H_2O in the pyrolysis chamber.

The original absorption spectrum of laser light absorbed by H_2O at wave numbers near 7185 and 7444 cm^{-1} was obtained directly by TDLAS, as shown in Figure S1.

The absorption spectrum is based on the Beer–Lambert Law, and the formula for absorbance can be derived from eq 1.

$$\alpha_\nu = PS(T)x_{abs}\phi_\nu L = -\ln\left(\frac{I_t}{I_0}\right) \tag{1}$$

In the equation, α_ν represents the absorbance at frequency ν, P is atmospheric pressure, $S(T)$ is the line strength that varies with temperature T, which is obtained by the HITRAN database, x_{abs} is the component concentration, ϕ_ν is the line shape function, L is the absorption path length, I_t is the absorbed light intensity, and I_0 is the incident light intensity.

Voigt line function is used to fit the absorption spectrum, and the relative wavenumber range of the DFB laser was calibrated with an F–P etalon prior to the experiment. The integrated absorbance A of the gas is given by the eq 2.

$$A = \int_{\nu_1}^{\nu_2} \alpha_\nu d\nu \tag{2}$$

where ν_1 and ν_2 are the wavenumber ranges of the absorption peaks.

The absorbances at 7185 and 7444 cm^{-1} are shown in Figure 2. Utilizing two absorption lines with different responses to temperature enables the measurement of gas temperature, known as the two-line thermometry method. The temperature can be obtained from the eq 3.

$$T = \frac{\frac{hc}{k}(E_1'' - E_2'')}{\ln\left(\frac{A_1}{A_2}\right) + \ln\left(\frac{S_1(T_0)}{S_2(T_0)}\right) + \left(\frac{hc}{k}\right)\left(\frac{E_2'' - E_1''}{T_0}\right)} \tag{3}$$

where h is the Planck constant ($h = 6.626 \times 10^{-34}$ J·s), k is the Boltzmann constant ($k = 1.38 \times 10^{-23}$ J/s), c is the speed of light in a vacuum ($c = 299792.458$ km/s), E_i'' is the lower-state energy level of the absorption line, A_i is the integrated absorbance of the target absorption peak, T_0 is the room temperature (296 K), and $S_i(T_0)$ is the line strength at temperature T_0.

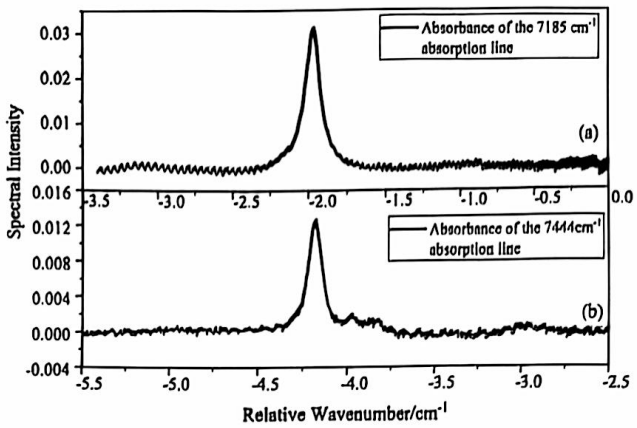

Figure 2. Absorption of (a) 7185 cm^{-1} and (b) 7444 cm^{-1} absorption line.

The average concentration of the target component (x_{abs}) along the detection path can be calculated as eq 4:

$$x_{abs} = \frac{A}{S(T)LP} \tag{4}$$

Through TDLAS laser in situ measurement, the temperature–time curve at a position of 1 mm above the biomass sample was obtained, as shown in Figure 3a. At the moment of laser heating, the biomass sample rapidly heats up and undergoes thermal decomposition, and the temperature at the measurement point quickly rises to reach a peak and then gradually decreases to room temperature. Comparing the temperature variation patterns at 1 mm above the sample during the pyrolysis process of samples with different moisture content, it was observed that both received and dry basis samples reached the maximum temperature during the dehydration and devolatilization stages. However, the maximum temperature of the received basis sample was higher than that of the dry basis sample during the pyrolysis process. Moisture plays a certain role in the pyrolysis process of

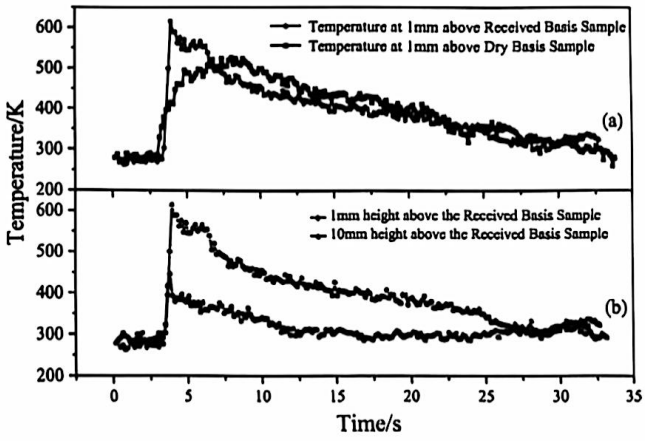

Figure 3. Temperature diagram at (a) 1 mm above the samples with different moisture and (b) different heights of biomass pyrolysis process.

https://doi.org/10.1021/acs.energyfuels.4c00154
Energy Fuels 2024, 38, 7929–7940

biomass, making the surface pyrolysis reaction of the received basis sample more intense.

The temperature variations at different heights above the received basis sample are illustrated in Figure 3b. Overall, the variation in temperature at 10 mm aligned with that at the 1 mm measurement point, but the peak temperature was noticeably lower than at the 1 mm position. When solid fuel particles were irradiated with a CO_2 laser, the surface temperature in the irradiation zone rapidly increased. Heat was then transferred and diffused from the irradiation zone to the interior of the sample particles. Some of the heat was lost through thermal radiation and convection, causing the temperature to decrease gradually with increasing distance from the measurement point.

The concentration of water vapor on the optical path 1 mm above the sample was measured using TDLAS technology, as depicted in Figure 4. During the pyrolysis process, two peaks in the release of water vapor were observed during the pyrolysis process, which lasted for approximately 20 s. Initially, the biomass rapidly released water vapor, causing a rapid increase in concentration that peaked before gradually declining. Subsequently, a second peak in water vapor release occurs, and finally, it gradually decreases to zero. The moisture release curve during the pyrolysis process of the dry basis sample was similar to that of the received basis sample but the peak concentration was smaller.

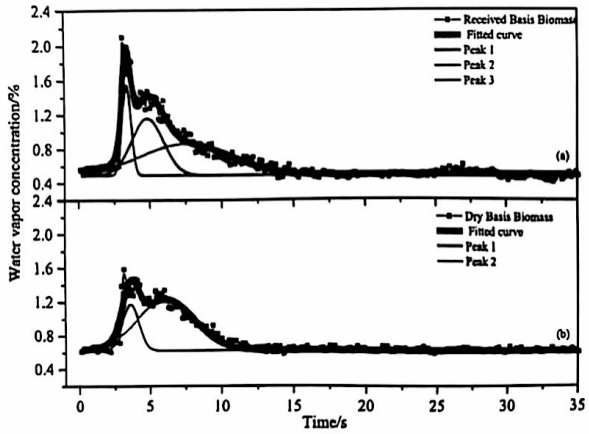

Figure 4. Water vapor release curves and split-peak fit (a) received basis sample; (b) dry basis sample.

The curve representing the generation of H_2O exhibits multiple peaks, with each peak and inflection point corresponding to a distinct reaction. The generation rate curves take the form of nonstandard Gaussian curves, which are fitted using Gaussian functions to resolve the spectral peaks. The water vapor releasing rate curve for the received sample was fitted with three Gaussian peaks, indicating that water vapor released from the biomass sample undergoes three reaction stages. The first peak corresponds to the removal of adsorbed water from the biomass pore structure during the dehydration and devolatilization stage. For the dry basis sample, two Gaussian peaks were observed, indicating that the release of water vapor from the sample occurs in two stages. The release of water vapor during biomass pyrolysis can be explained by the scission of aliphatic hydroxide groups and the binding with hydrogen radicals.[33] This accounts for the water vapor release peaks observed in the dry basis sample as well as the second and third release peaks observed in the received basis sample.

Methane is one of the most important products in the biomass pyrolysis conversion process. The CH_4 concentration above the surface of the biomass sample was measured at positions 1 and 10 mm using the absorption line at 1654 nm. The calculation method for the CH_4 concentration is consistent with that for H_2O, and its temporal variation is shown in Figure 5. During the initial stage of the pyrolysis process, the CH_4 concentration rapidly increased above the 1 mm position of the biomass sample, reaching a peak concentration before gradually decreasing. The release rate decreased overall until it reached zero. As the spatial height increased, the peak concentration of methane release also decreased. The CH_4 release patterns for dry basis and received

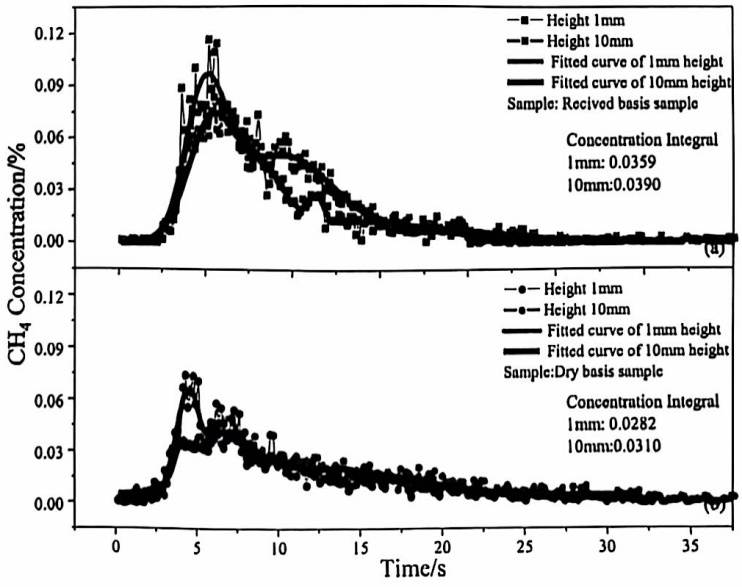

Figure 5. Methane generation curves for samples with different moisture content (a) received basis sample; (b) dry basis sample.

https://doi.org/10.1021/acs.energyfuels.4c00154
Energy Fuels 2024, 38, 7929−7940

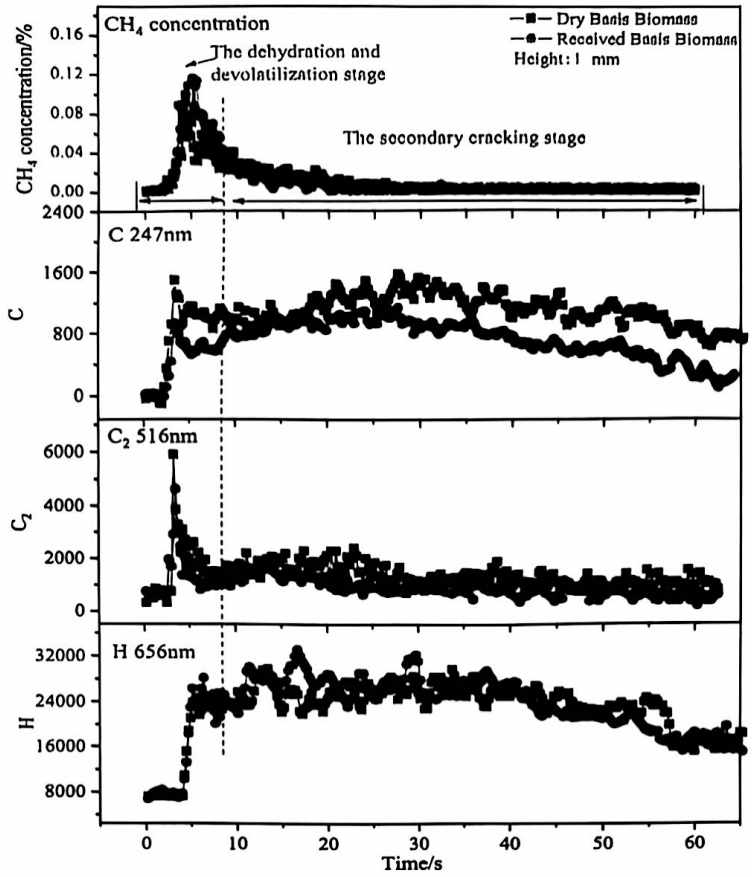

Figure 6. Release curves of methane and related spectral lines (C, H, C_2) at 1 mm above the samples.

basis samples are similar. However, during the dehydration and devolatilization stages, the peak concentration of CH_4 released from the received basis sample was higher.

The integration of the methane concentration over the entire pyrolysis reaction time provides its total yield, which enables a comprehensive understanding of the biomass pyrolysis behavior and product formation patterns. By comparing the cumulative methane production, we can evaluate the impact of the pyrolysis conditions on methane generation. Furthermore, by comparing cumulative methane production at different positions, we can infer potential reaction pathways. For the received biomass sample, the integration resulted in 0.0359 at 1 mm height and 0.0390 at 10 mm height, indicating an increase of 0.0031. The integration for the dry basis sample was 0.0282 at 1 mm height and 0.0310 at 10 mm height, indicating an increase of 0.0028. The integral of methane concentration at the 10 mm position was higher than that at the 1 mm position. This suggests that in addition to the methane generated by bond breaking and desorption on the solid fuel surface, a small amount of methane was also produced in the gas phase space. This could be due to the secondary cracking of unstable large molecules, such as tar, under heated conditions, resulting in the production of smaller molecules, including methane.[34] During the pyrolysis process, the received basis sample exhibited a higher rate of methane release and a greater total amount of methane released. This indicates that, with the presence of moisture, the received basis sample possessed an enhanced conversion rate of large-molecule tars, resulting in the production of a larger quantity of smaller molecule gases such as methane.

3.2. Analysis of Characteristic Elements and Groups of Gas Phase Products by LIBS. To gain a further understanding of the characteristics of volatile products during the rapid pyrolysis of biomass eucalyptus, LIBS technology was employed to collect transformation-related feature spectrum such as C 247 nm, H 656 nm, C_2 516 nm, etc., at spatial heights of 1 mm and 10 mm above the surface of the biomass sample. Combining the release patterns of the characteristic elements with those of CH_4 obtained by TDLAS allows for the qualitative identification of organic compounds produced during pyrolysis. The full LIBS spectrum of the biomass sample after 5 s of the pyrolysis process is shown in Figure S2. Temperature has some effects on the LIBS spectrum, but in our previous study, we found that the intensity ratios of the different characteristic elemental peaks varied very little with temperature.[35] The characteristic spectral line intensity ratios can be used to eliminate the impact of temperature on the accuracy of the spectra.

The characteristic spectrum of the C element originated from various gases containing carbon elements in the volatile fraction. The intensity ratio of the characteristic spectrum between C and H elements (C/H) can qualitatively characterize the carbon chain length of the measured substance, indicating the size of the molecular weight of the organic compounds.

However, unlike atomic carbon spectra, the spectrum of C_2 is affected not only by the concentration of the target component but also by the types of organic compounds present in the measured gas. In our previous research,[36] it has been shown that the emission lines of neutral atomic carbon

https://doi.org/10.1021/acs.energyfuels.4c00154
Energy Fuels 2024, 38, 7929−7940

are 2–3 times larger than those of diatomic species such as C_2. The molecular bands of C_2 may directly arise from samples containing diatomic structures, such as single bond C–C or double bond C=C. Mousavi et al.[37] also pointed out that the main reasons for the formation of C_2 molecules are the direct fragmentation of organic compounds releasing C_2 and the carbon atoms integration of compounds under the effect of plasma. Therefore, the main sources of C_2 include (1) fragmentation of gases or macromolecular components with more than two carbon atoms; (2) reforming of carbon atoms from methane.

Based on this feature, we utilize the C_2 spectrum and the C/H ratio, which characterizes the molecular weight of the substance, to achieve recognition of organic products and jointly characterize the evolution of organic products in the gas phase fraction.

During the pyrolysis process, variations in element distribution arise due to differences in component distribution. Figure 6 illustrates the release curves of methane and related spectral lines (C, H, C_2) at 1 mm height above the samples during the pyrolysis process. Further details regarding the mentioned parameters at 10 mm above the samples can be found in Figure S3. The transformation pathways of pyrolysis components were analyzed based on the temporal and spatial changes in various characteristic spectra. As shown in Figure 7,

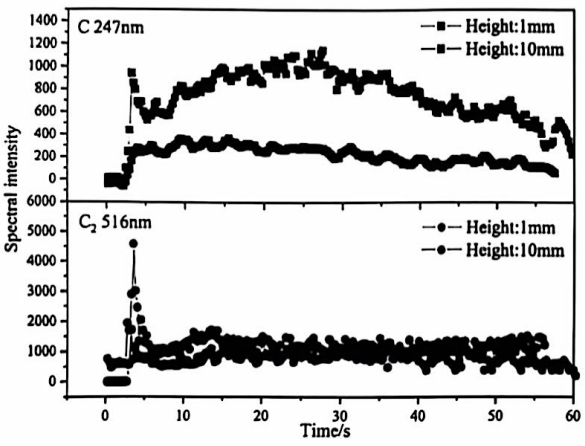

Figure 7. C and C_2 release curves at 1 mm and 10 mm above the received basis samples.

there are two release peaks of both C atoms and C_2 groups 1 mm above the sample, indicating that a large amount of carbon-containing material was released in the two stages of pyrolysis. The first release peaks of the C and C_2 spectra were concentrated in the stage of dehydration and devolatilization. These peaks appeared rapidly and declined within the first 10 s. The second release peaks appeared in the second cracking stage, which occurred after 10 s until the end of the pyrolysis process. The peak intensity of the C spectrum showed little difference in both stages. However, during the dehydration and devolatilization stages, the C_2 spectrum shows a strong and brief intensity, while in the secondary cracking stage, the C_2 spectrum intensity is weaker but persists until the end of the pyrolysis process. This indicates a difference in the types of organic compounds released during the two stages.

The LIBS spectrum collects elements from biomass pyrolysis products in situ. However, the identification of organic compound types cannot be achieved solely based on the characteristic spectrum of C and C_2. By combining the CH_4 emission characteristics measured by TDLAS, it is possible to qualitatively differentiate the types of organic compounds in the pyrolysis products. The emission peak of methane coincides with the first emission peaks of C and C_2, indicating that during the dehydration and devolatilization stage, the significant emission of carbon-containing small molecular gases, such as methane, was the main contributor to the formation of the first emission peaks of C and C_2. In the secondary cracking stage, the methane emission was relatively low, while C and C_2 exhibited a second emission peak. This indicates that the second emission peak in this stage is contributed by other types of organic compounds. The sources of the second emission peak are diverse and may be attributed to the small amount of small molecular gases, such as ethylene and acetylene, generated from the cracking of large molecular tars.

Additionally, it was observed that the moisture-rich basis samples released more methane during the pyrolysis process. However, their C and C_2 characteristic peak intensities were lower than those of the dry basis samples. This phenomenon may be influenced by the tar generated during the biomass pyrolysis process. During the pyrolysis process of the received basis samples, the concentration of moisture played a significant role in the cracking of tar, which led to the generation of small molecular gases. In contrast, the dry basis samples released less moisture, making it difficult to crack the accumulation of large molecular tar above the sample surface, resulting in stronger C and C_2 spectrum intensities.

Figure 7 shows the pattern of C and C_2 spectra at different heights above the received basis samples. The C spectrum peaked at the start of the pyrolysis process and gradually decreased at a height of 10 mm above the samples. In contrast, the C_2 spectrum distinctly reveals two release peaks, further illustrating differences in the types and sources of organic compounds during the dehydration and devolatilization stage and the secondary cracking stage at 10 mm. The intensity of the C and C_2 spectrum at the position 10 mm above the sample surface is significantly lower than that at 1 mm above the sample. This may be due to the fact that the organic compounds at 1 mm above the sample surface were more easily excited to produce C and C_2 spectra, while at 10 mm, the excitation of the spectrum from organic compounds was more difficult. During the pyrolysis process, large molecular tars and small organic gases coalesced, and they are the main substances forming the C and C_2 spectrum. Compared to large molecular tars, noncondensable small molecular gases have stable structures and are more difficult to excite to form C and C_2 spectra. The accumulation of tar near the sample surface is the primary reason for the stronger C and C_2 spectrum at 1 mm above the sample.

To investigate the spatial variation of organic compounds during the dehydration and devolatilization stages at 1 mm and 10 mm above the sample surface. Figure 8 shows a comparison of the spatial distribution of the C/H ratio. At 1 mm above the sample surface, two peaks in the C/H ratio were observed. The peak for the dehydration and devolatilization stages was shorter, while the peak for the secondary cracking stage was smoother and longer. During the initial stage of pyrolysis in the dehydration and devolatilization stages, small molecular hydrocarbons such as methane are released from the sample surface, forming the first peak. As it enters the secondary

https://doi.org/10.1021/acs.energyfuels.4c00154
Energy Fuels 2024, 38, 7929–7940

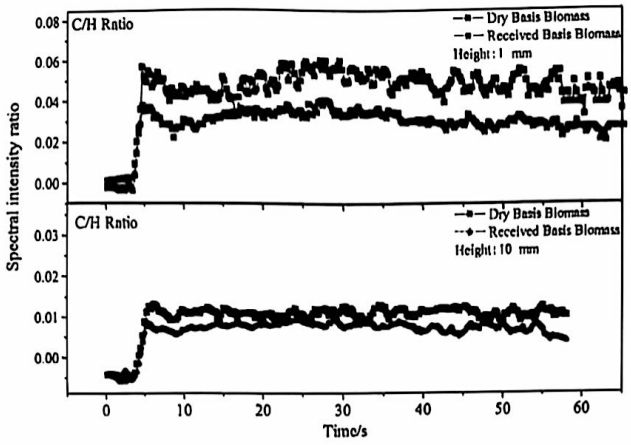

Figure 8. Comparison of the C/H ratio in samples with different moisture contents.

cracking stage, large molecular tars continuously crack to produce noncondensable gases with two or more carbons, forming the second peak. The C/H ratio at 1 mm above the sample surface was significantly higher than at 10 mm. This is because near the sample surface at 1 mm, large molecular tars can be detected, and unstable large molecular tars gradually undergo thermal cracking during diffusion. At 10 mm, only methane and small molecular gases produced by cracking can be detected. The C/H ratio of pyrolysis products from the dry basis sample was higher than that of the received basis sample, whether at 1 mm or 10 mm above the sample. The results show that the tar conversion rate was lower for the dry basis sample, which led to a higher accumulation of large molecular tars and a higher C/H ratio. In contrast, the received basis sample released more water vapor, promoting tar cracking and resulting in a higher tar conversion rate and a lower C/H ratio.

3.3. Analysis of the Molecular Structure of Biomass Char by Raman. LIBS conducts elemental analysis of gaseous pyrolysis products from an atomic emission spectroscopy perspective, while TDLAS quantitatively measures H_2O and CH_4 in gaseous pyrolysis products from a molecular absorption spectroscopy viewpoint. However, in situ spectral detection cannot further analyze the molecular structure of biomass surface char. Therefore, Raman spectroscopy is introduced to complementarily study the structure of active functional groups in pyrolysis char, which has been widely applied for the ex situ characterization of products (char and ash) as well as for in situ diagnostics during reactions.[33] The molecular structure of biomass surface char changes with the progress of the pyrolysis process, and the activity and detachment of functional groups on surface char are closely related to the types and yields of gaseous products. Therefore, we conducted Raman spectroscopy analysis on samples from different pyrolysis stages and compared the CH_4 release patterns with the changes in surface char structure.

Through pre-experiments based on TDLAS and LIBS spectra measurements, we found that both spectra peaked rapidly within the first 5 s of pyrolysis. Based on the spectrum results, the pyrolysis process of biomass can be divided into two stages: the first 10 s is the stage of dehydration and devolatilization, while the period after 10 s until the end of pyrolysis is the stage of secondary decomposition. Therefore, samples were taken at 5 and 10 s, and their intermediate moment of 7.5 s. Samples 1−3 represented the changes in surface char during the dehydration and devolatilization stage. Since CH_4 generation mostly ceased after 15 s of pyrolysis, the fourth sampling was performed to observe variations in the molecular structure of the surface char during the secondary decomposition stage. Finally, sample 5 was used to characterize the biomass char structure after pyrolysis was completed. By sampling at specific intervals during pyrolysis, we could monitor the changing trend of the molecular structure of char throughout the process. Samples of biomass char were collected at different time intervals during the pyrolysis process and labeled as samples 1−5 based on the time. Table 2 shows the time intervals at which the samples were collected.

Table 2. Biomass Sample Numbers and Sampling Times

sample number	1	2	3	4	5
sampling time (s)	5	7.5	10	15	complete pyrolysis

The Raman spectrum of biomass is typically the result of the convolution of multiple carbon structure bands, which requires deconvolution. Researchers have classified the Raman spectrum of biomass char in the 800−1800 cm^{-1} range. The Raman spectrum of each sample was normalized based on the central spectral positions of the bands. Then the spectra were baseline-corrected and peak-fitted using Peakfit software. Gaussian peak fitting was applied to the Raman total peak in the 800−1800 cm^{-1} range, with each peak representing typical structures in biomass.

The Raman spectrum of biomass char is mainly characterized by two bands, approximately 1350−1370 and 1580−1600 cm^{-1}, representing the D peak of sp^2 carbon structures, indicating structural defects, and the G peak representing graphite carbon structures, respectively.[38] By analyzing the overlap between the D band and the G band, as well as the shoulders, important information about the structural characteristics of the biomass char can be captured. The overlapping region between the D and G bands can be divided into three parts: G_R (1540 cm^{-1}), V_L (1465 cm^{-1}), and V_R (1380 cm^{-1}). These represent characteristic structures of different amorphous carbons and the semicircular vibrations of aromatic rings. The Raman spectrum including prominent peaks such as the G, D, V_R, G_R, and V_L bands are shown in Figure S4.

The relative intensity ratio of the D band to the G band, known as I_D/I_G, is often used to characterize the structural features and defect levels of materials.[38] Generally, samples with higher I_D/I_G ratios tend to exhibit higher defect content and amorphous structures, leading to an increased surface area and more active sites exposed on the surface. Therefore, some studies suggest that char with higher I_D/I_G ratios tends to have more disordered carbon crystal structures and higher char reactivity.[39] Conversely, the ratio of I_D/I_G decreases as the degree of graphitization increases.

Figure 9 illustrates a comparison between the I_D/I_G ratio and methane evolution curve at different pyrolysis stages of biomass samples, revealing a similar trend between the two. The surface char activity of biomass was positively correlated with the methane concentration in the pyrolysis gas phase, suggesting that most of the methane production was due to surface reactions on the biomass. During the dehydration and devolatilization stage, the I_D/I_G ratio rapidly increased, indicating that the carbon structure of the char becomes disordered, and the reactivity of biomass char increased. Intense surface reactions occurred during this pyrolysis stage, resulting in the significant release of volatile gases, including

https://doi.org/10.1021/acs.energyfuels.4c00154
Energy Fuels 2024, 38, 7929−7940

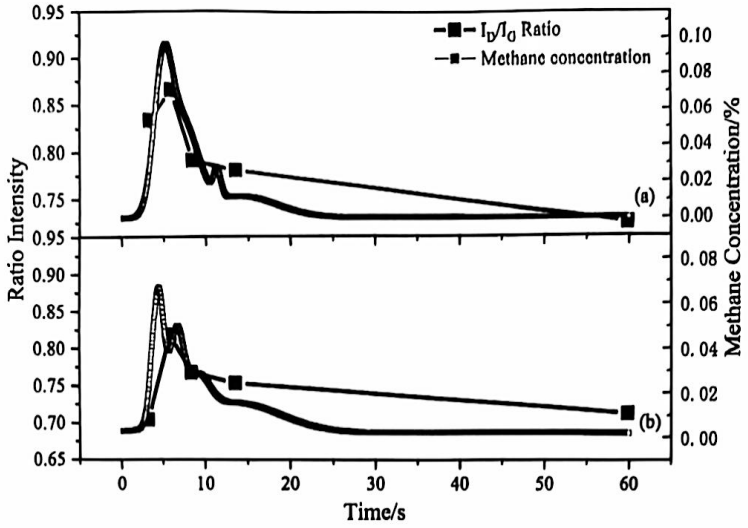

Figure 9. I_D/I_G ratio of the biomass char Raman spectrum and the methane evolution curve at 1 mm above the sample surface. (a) Received basis sample; (b) dry basis sample.

methane. In the secondary cracking stage, there was a noticeable decrease in the I_D/I_G ratio. Compared with the dehydration and devolatilization stage, the secondary cracking stage was dominated by gas phase reactions, resulting in fewer structural changes in biomass char. As a result, the surface activity gradually decreased and the aromaticity of the char increased, indicating a more stable chemical structure on the char surface.

The I_D/I_G ratios of samples with varying moisture contents exhibit a similar trend, initially increasing and then decreasing. During the dehydration and devolatilization stage, the received basis sample shows a higher I_D/I_G ratio and methane concentration, indicating greater reactivity of the received basis biomass char. The increase in porosity and surface area resulting from the removal of free water from the sample's porous structure may be responsible for the intensified pyrolysis reactions and enhanced reactivity of the formed surface char, ultimately promoting the release of volatile gases.

The bands located between the D peak and G peak (G_R, V_L, and V_R) contain valuable structural information. The G_R, V_L, and V_R bands represent smaller aromatic ring polymerization degrees (3–5 aggregated aromatic rings) in amorphous carbon, such as submethyl or methyl structures. On the other hand, the D peak mainly represents the defect structure of carbon materials with highly regularized structures (more than 6 benzene rings). The proportion of large aromatic rings to small aromatic rings in char can be represented by $I_D/(I_{GR} + I_{VL} + I_{VR})$, which is the peak area ratio of the D peak to ($G_R + V_L + V_R$) peaks. Figure 10a shows the trends of $I_D/(I_{GR} + I_{VL} + I_{VR})$ and Figure 10b shows integrated methane concentration for both the received basis sample and the dry basis sample over the pyrolysis process. The $I_D/(I_{GR} + I_{VL} + I_{VR})$ and integrated methane concentrations showed a similar trend, rapidly increasing during the dehydration and devolatilization stage and showing a smaller increase during the secondary cracking stage. This indicates that during the dehydration and devolatilization stage, small aromatic rings were continuously consumed or rapidly condensed into large ones. Methane formed as methyl and methylene carbon structures continuously detached. In the secondary cracking stage, this rate slowed down, and the chemical structure of biomass char

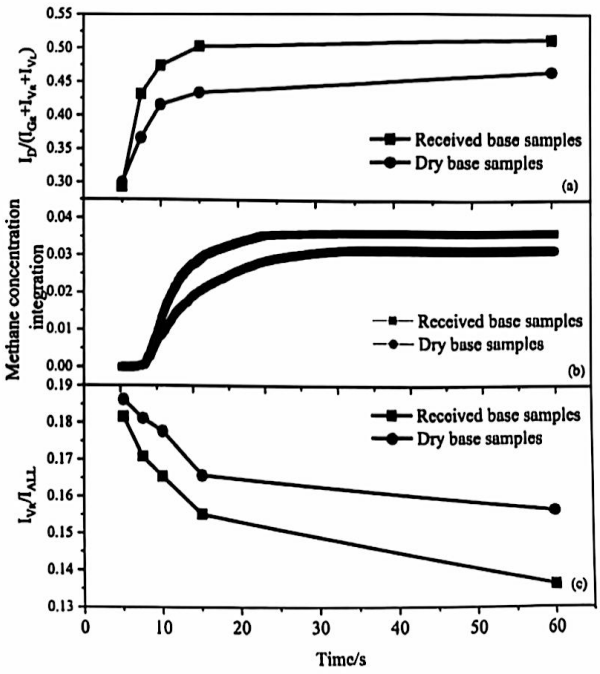

Figure 10. Characteristic parameters of biomass pyrolysis (a) $I_D/(I_{GR} + I_{VL} + I_{VR})$ (b) methane generation integral curve (c) I_{VR}/I_{all}.

became more regular. In the same pyrolysis reaction stage, the received basis sample with a higher moisture content had a larger $I_D/(I_{GR} + I_{VL} + I_{VR})$. Moisture promoted the detachment of smaller aromatic structures, resulting in the generation of volatile gases such as methane. It also facilitated the condensation of these structures into larger molecules with six or more aromatic rings. As a result, the sample exhibited a decreasing proportion of small aromatic structures and an increasing proportion of large aromatic structures, leading to a more stable chemical structure of biomass char.

Figure 10c shows the variation curve of I_{VR}/I_{all} for samples with different moisture contents during the pyrolysis stage. The production of methane during biomass pyrolysis is strongly linked to the methylene functional groups. The V_R

https://doi.org/10.1021/acs.energyfuels.4c00154
Energy Fuels 2024, 38, 7929–7940

peak at 1380 cm^{-1} represents the fundamental vibration of the methylene functional groups. By comparison of the proportion of the V_R peak area to the total peak area in different samples, the qualitative analysis of changes in the content of methylene functional groups in biomass char can be determined. The continuous decrease in methylene functional groups during the pyrolysis process was proportional to the total amount of methane released. In the dehydration and devolatilization stage, a large amount of methylene groups detached, and the released methyl groups combined with hydrogen radicals to generate methane, leading to a significant release of methane during this stage. During the secondary cracking stage, the surface char activity decreased, resulting in a slower rate of methylene group detachment. As a result, the production of methane decreased significantly. When comparing biomass samples with varying moisture content, the residual content of methyl functional groups in the received basis sample was lower than that in the dry basis sample at the same time. Prior to pyrolysis, the amount of methyl functional groups in the dry basis sample was equivalent to that in the received basis sample. As pyrolysis commences, the heightened surface reaction activity facilitates the detachment of methyl functional groups, thereby increasing methane production. Upon entering the secondary cracking stage, with the decreasing rate of methyl functional group detachment, the rate of methane generation gradually decreased.

3.4. Integrated Analysis of Multispectral Results. The biomass pyrolysis process was characterized by using a multispectral association in various perspectives. TDLAS and LIBS were employed to characterize the released gas phase products (CH_4 and H_2O) and their characteristic elements (C, C_2, H), while Raman spectroscopy was utilized to characterize the solid phase biomass char structure. The pyrolysis process of biomass eucalyptus can be divided into a dehydration and devolatilization stage and a secondary cracking stage by analyzing the release patterns of gas products.

During the dehydration and devolatilization stages, the reactivity of biomass char increases, leading to significant detachment of functional groups such as methylene, which subsequently combines with hydrogen radicals to generate CH_4. The extensive release of CH_4 during this stage can be monitored using TDLAS, while the first release peaks of characteristic elements such as C and C_2, as detected by LIBS, primarily originate from volatile gases such as CH_4. Samples with a higher moisture content exhibit higher reactivity on their surface, which promotes the detachment of methylene functional groups. As a result, they release a higher concentration of methane compared with dry basis samples.

During the secondary cracking stage, the reactivity of the biomass surface char gradually decreases, resulting in a reduction in the detachment rate of functional groups and stabilization of the chemical structure. Consequently, the production of volatiles, such as CH_4, decreases. This stage is dominated by gas phase reactions. The C/H ratio of 1 mm above the biomass samples is larger than that of 10 mm above the samples, indicating that large molecules of tar are gathered near the surface of the samples. By comparing the cumulative methane production at 1 and 10 mm above the samples, it is observed that the accumulation is higher at 10 mm. It suggested that in addition to methane generation through solid fuel surface cleavage during the dehydration and devolatilization stage, a small amount of methane is also produced in the gas phase. This methane may originate from the cracking of unstable tar during diffusion. The second peak in the characteristic spectra of C and C_2 measured by LIBS may originate from ethylene and other small molecule gases generated during tar cracking. The increase in methane in the gas phase of the received basis samples indicates that the release of water vapor may facilitate the cracking process of large molecules.

It is well known that establishing a mathematical model of fuel pyrolysis requires a comprehensive description of the relevant physical and chemical processes, including thermodynamics, chemical kinetics, and component transport. To predict the reaction rates and product formation rates of fuel pyrolysis, it is necessary to develop a multistep kinetic model of fuel devolatilization.[40] The spatiotemporal distribution data obtained from experimental measurements can provide important clues for elucidating the mechanism of pyrolysis reactions, inferring possible reaction pathways and intermediate products. In our experiments, TDLAS was used to realize the quantitative analysis of the gas phase products (CH_4 and H_2O) of biomass pyrolysis, and LIBS was used for the qualitative analysis of the characteristic elements (C, H, C_2) of the gas phase products. By analyzing the spatiotemporal distribution of products CH_4 and characteristic elements C and C_2 in experiments, it is inferred that the kinetic model of pyrolysis must consider the cracking reactions of tar in the gas phase. The model requires fuel characterization based on proximate analysis and ultimate analysis, as shown in Table 1. Kinetic models involving multiple species and reactions are then used to describe the products released during the devolatilization stages. Model calculations can predict the release characteristics of major pyrolysis products (such as CH_4, H_2O, CO, H_2, etc.). The experimental analysis can be used to compare with model predictions, and the kinetic parameters of each reaction can be adjusted based on the experimental results to improve the accuracy of the model.

4. CONCLUSIONS

In this work, the spatiotemporal distribution characteristics of gas and solid products during the pyrolysis of eucalyptus biomass were revealed by using a multispectral association method, including TDLAS, LIBS, and Raman spectroscopy. The gas phase products H_2O and CH_4 were quantitatively measured, and the organic compounds generated during pyrolysis were qualitatively identified. Furthermore, we established correlations between the molecular structure of the solid biomass char and the spatiotemporal release pattern of the gas phase pyrolysis products. It was found that in the devolatilization stage, the surface reactivity of biomass char was increased and the functional groups were detached, resulting in the release of volatiles including CH_4. The secondary pyrolysis stage is dominated by gas reaction, and the tar in the gas phase cracks into smaller molecular gas. The moisture content in the samples enhances the reactivity of biomass char, and the release of water vapor may facilitate the cracking process of large molecules. Our work investigated the gas phase product formation of eucalyptus pyrolysis from both molecular and atomic perspectives, providing a database for the establishment of kinetic models of biomass pyrolysis.

■ ASSOCIATED CONTENT

Supporting Information

The Supporting Information is available free of charge at https://pubs.acs.org/doi/10.1021/acs.energyfuels.4c00154.

https://doi.org/10.1021/acs.energyfuels.4c00154
Energy Fuels 2024, 38, 7929−7940

TDLAS-H_2O original absorption spectrum, full LIBS spectrum of the biomass sample during pyrolysis, release curves of methane and related spectral lines (C, H, C_2) at 10 mm above the samples, and Raman spectrum and peak splitting diagram of the received base sample 1 (PDF)

AUTHOR INFORMATION

Corresponding Author

Meirong Dong − *School of Electric Power, South China University of Technology, Guangzhou, Guangdong 510640, China; Guangdong Province Engineering Research Center of High Efficient and Low Pollution Energy Conversion, Guangzhou, Guangdong 510640, China;* orcid.org/0000-0003-3247-1918; Email: epdongmr@scut.edu.cn

Authors

Xiao Lin − *School of Electric Power, South China University of Technology, Guangzhou, Guangdong 510640, China; Guangdong Province Engineering Research Center of High Efficient and Low Pollution Energy Conversion, Guangzhou, Guangdong 510640, China*

Wei Nie − *AnHui Institute of Optics and Fine Mechanics, HeFei Institutes of Physical Sciences, Chinese Academy of Sciences, Hefei 230031, China*

Gangfu Rao − *School of Electric Power, South China University of Technology, Guangzhou, Guangdong 510640, China; Guangdong Province Engineering Research Center of High Efficient and Low Pollution Energy Conversion, Guangzhou, Guangdong 510640, China*

Jidong Lu − *School of Electric Power, South China University of Technology, Guangzhou, Guangdong 510640, China; Guangdong Province Engineering Research Center of High Efficient and Low Pollution Energy Conversion, Guangzhou, Guangdong 510640, China;* orcid.org/0000-0003-3351-0456

Complete contact information is available at: https://pubs.acs.org/10.1021/acs.energyfuels.4c00154

Author Contributions

X.L. was responsible for conceptualization, methodology, investigation, and writing the original draft; M.D. was responsible for supervision, writing, reviewing, editing, and resources; W.N. was responsible for supervision, reviewing, editing; G.R. was responsible for investigation; and J.L. was responsible for reviewing, editing, and resources.

Funding

The research was supported by the National Natural Science Foundation of China [No. 51976064, 52376107, 62105104]; the Guangdong Basic and Applied Basic Research Foundation [2022A1515010709]; the Fundamental Research Funds for the Central Universities [2022ZFJH04] and the Science and Technology Planning Project of Guangzhou [202102020726].

Notes

The authors declare no competing financial interest.

ACKNOWLEDGMENTS

The research acknowledges the support from the Guangdong Province Key Laboratory of Efficient and Clean Energy Utilization (2013A061401005).

REFERENCES

(1) Chen, H.; Liu, Z.; Chen, X.; Chen, Y.; Dong, Z.; Wang, X.; Yang, H. Comparative pyrolysis behaviors of stalk, wood and shell biomass: Correlation of cellulose crystallinity and reaction kinetics. *Bioresour. Technol.* **2020**, *310*, 123498.

(2) Jalan, R. K.; Srivastava, V. K. Studies on pyrolysis of a single biomass cylindrical pellet-kinetic and heat transfer effects. *Energy Convers. Manage.* **1999**, *5* (40), 467−494.

(3) El Naggar, A. M. A.; El Sayed, H. A.; Elsalamony, R. A.; Elrazak, A. A. Biomass to fuel gas conversion through a low pyrolysis temperature induced by gamma radiation: an experimental and simulative study. *RSC advances.* **2015**, *5* (95), 77897−77905.

(4) Wu, L.; Ni, J.; Zhang, H.; Yu, S.; Wei, R.; Qian, W.; Chen, W.; Qi, Z. The composition, energy, and carbon stability characteristics of biochars derived from thermo-conversion of biomass in air-limitation, CO_2, and N_2 at different temperatures. *Waste Management.* **2022**, *141*, 136−146.

(5) Collard, F. X.; Blin, J. A review on pyrolysis of biomass constituents: Mechanisms and composition of the products obtained from the conversion of cellulose, hemicelluloses and lignin. *Renewable and Sustainable Energy Reviews.* **2014**, *38*, 594−608.

(6) Werner, K.; Pommer, L.; Broström, M. Thermal decomposition of hemicelluloses. *Journal of Analytical and Applied Pyrolysis.* **2014**, *110*, 130−137.

(7) Quan, C.; Gao, N.; Song, Q. Pyrolysis of biomass components in a TGA and a fixed-bed reactor: Thermochemical behaviors, kinetics, and product characterization. *Journal of Analytical and Applied Pyrolysis.* **2016**, *121*, 84−92.

(8) Pimenta, A. S.; Monteiro, T. V. D. C.; Fasciotti, M.; Braga, R. M.; Souza, E. C. D.; Lima, K. M. G. D. Fast pyrolysis of trunk wood and stump wood from a Brazilian eucalyptus clone. *Industrial Crops and Products.* **2018**, *125*, 630−638.

(9) Kai, X.; Li, R.; Yang, T.; Shen, S.; Ji, Q.; Zhang, T. Study on the co-pyrolysis of rice straw and high density polyethylene blends using TG-FTIR-MS. *Energy Conversion and Management.* **2017**, *146*, 20−33.

(10) Yan, R.; Yang, H.; Chin, T.; Liang, D. T.; Chen, H.; Zheng, C. Influence of temperature on the distribution of gaseous products from pyrolyzing palm oil wastes. *Combust. Flame* **2005**, *142* (1−2), 24−32.

(11) Huang, Y.; Sekyere, D. T.; Zhang, J.; Tian, Y. Fast pyrolysis behaviors of biomass with high contents of ash and nitrogen using TG-FTIR and Py-GC/MS. *Journal of Analytical and Applied Pyrolysis.* **2023**, *170*, 105922.

(12) Trubetskaya, A.; Souihi, N.; Umeki, K. Categorization of tars from fast pyrolysis of pure lignocellulosic compounds at high temperature. *Renewable Energy.* **2019**, *141*, 751−759.

(13) Montiano, M. G.; Fernández, A. M.; Díaz-Faes, E.; Barriocanal, C. Tar from biomass/coal-containing briquettes Evaluation of PAHs. *Fuel.* **2015**, *154*, 261−267.

(14) Li, X.; Hayashi, J.; Li, C. FT-Raman spectroscopic study of the evolution of char structure during the pyrolysis of a Victorian brown coal. *Fuel.* **2006**, *85* (12−13), 1700−1707.

(15) Keown, D. M.; Li, X.; Hayashi, J.; Li, C. Evolution of biomass char structure during oxidation in O_2 as revealed with FT-Raman spectroscopy. *Fuel Process. Technol.* **2008**, *89* (12), 1429−1435.

(16) Surup, G. R.; Nielsen, H. K.; Heidelmann, M.; Trubetskaya, A. Characterization and reactivity of charcoal from high temperature pyrolysis (800−1600 °C). *Fuel* **2019**, *235*, 1544−1554.

(17) Zhang, J.; Zhang, K.; Huang, J.; Feng, Y.; Yellezuome, D.; Zhao, R.; Chen, T.; Wu, J. Synergistic effect and volatile emission characteristics during co-combustion of biomass and low-rank coal. *Energy.* **2024**, *289*, 130015.

(18) Sepman, A.; Thorin, E.; Ögren, Y.; Ma, C.; Carlborg, M.; Wennebro, J.; Broström, M.; Wiinikka, H.; Schmidt, F. M. Laser-based detection of methane and soot during entrained-flow biomass gasification. *Combust. Flame* **2022**, *237*, 111886.

(19) Sepman, A.; Ögren, Y.; Wennebro, J.; Wiinikka, H. Simultaneous diagnostics of fuel moisture content and equivalence ratio during combustion of liquid and solid fuels. *Applied Energy.* **2022**, *324*, 119731.

(20) Wu, Q.; Wang, F.; Li, M.; Yan, J.; Cen, K. Simultaneous In-Situ Measurement of Soot Volume Fraction, H_2O Concentration, and Temperature in an Ethylene/Air Premixed Flame Using Tunable Diode Laser Absorption Spectroscopy. *Combustion science and technology.* **2017**, *189* (9), 1571−1590.
(21) Wu, W.; Axelbaum, R. L. Interpreting diffusion flame structure by simultaneous mixture fraction and temperature measurements using optical and acoustic signals from laser-induced plasmas. *Proceedings of the Combustion Institute.* **2021**, *38* (1), 1665−1674.
(22) He, Y.; Zhu, J.; Li, B.; Wang, Z.; Li, Z.; Aldén, M.; Cen, K. In-situ Measurement of Sodium and Potassium Release during Oxy-Fuel Combustion of Lignite using Laser-Induced Breakdown Spectroscopy: Effects of O_2 and CO_2 Concentration. *Energy & Fuels.* **2013**, *27* (2), 1123−1130.
(23) Li, S.; Dong, M.; Luo, F.; Li, W.; Wei, L.; Lu, J. Experimental investigation of combustion characteristics and NOx formation of coal particles using laser induced breakdown spectroscopy. *Journal of the Energy Institute.* **2020**, *93* (1), 52−61.
(24) Kotzagianni, M.; Yuan, R.; Mastorakos, E.; Couris, S. Laser-induced breakdown spectroscopy measurements in turbulent methane flames. In *52nd Aerospace Sciences Meeting*, 2014; pp 1−12.
(25) Kotzagianni, M.; Kakkava, E.; Couris, S. Laser-Induced Breakdown Spectroscopy (LIBS) for the Measurement of Spatial Structures and Fuel Distribution in Flames. *Appl. Spectrosc.* **2016**, *70* (4), 627−634.
(26) Lee, J.; Bong, C.; Yoo, J.; Bak, M. S. Combined use of TDLAS and LIBS for reconstruction of temperature and concentration fields. *Optics Express.* **2020**, *28* (14), 21121−21133.
(27) Weng, W.; Aldén, M.; Li, Z. Insight into KOH and KCl release behavior of burning wood and straw pellets using quantitative in situ optical measurements. *Proceedings of the Combustion Institute.* **2023**, *39* (3), 3239−3248.
(28) Deguchi, Y.; Noda, M.; Fukuda, Y.; Ichinose, Y.; Endo, Y.; Inada, M.; Abe, Y.; Iwasaki, S. Industrial applications of temperature and species concentration monitoring using laser diagnostics. *Meas. Sci. Technol.* **2002**, *13* (10), R103−R115.
(29) Qu, M.; Ishigaki, M.; Tokuda, M. Ignition and combustion of laser-heated pulverized coal. *Fuel.* **1996**, *75* (10), 1155−1160.
(30) Ao, W.; Wang, Y.; Li, H.; Xi, J.; Liu, J.; Zhou, J. Effect of Initial Oxide Layer on Ignition and Combustion of Boron Powder. *Propellants, Explosives, Pyrotechnics.* **2014**, *39* (2), 185−191.
(31) Nagali, V.; Chou, S. I.; Baer, D. S.; Hanson, R. K.; Segall, J. Tunable diode-laser absorption measurements of methane at elevated temperatures. *Appl. Opt.* **1996**, *35* (21), 4026−4032.
(32) Mihalcea, R. M.; Baer, D. S.; Hanson, R. K. Diode laser sensor for measurements of CO, CO_2, and CH_4 in combustion flows. *Appl. Opt.* **1997**, *36* (33), 8745−8752.
(33) Xu, J.; He, Q.; Xiong, Z.; Yu, Y.; Zhang, S.; Hu, X.; Jiang, L.; Su, S.; Hu, S.; Wang, Y.; Xiang, J. Raman Spectroscopy as a Versatile Tool for Investigating Thermochemical Processing of Coal, Biomass, and Wastes: Recent Advances and Future Perspectives. *Energy & Fuels.* **2021**, *35* (4), 2870−2913.
(34) Pattanayak, S.; Hauchhum, L.; Loha, C.; Sailo, L.; Mishra, L. Experimental investigation on pyrolysis kinetics, reaction mechanisms and thermodynamic parameters of biomass and tar in N2 atm. *Sustainable Energy Technologies and Assessments.* **2021**, *48*, 101632.
(35) Li, S.; Dong, M.; Cheng, L.; Luo, F.; Zhao, W.; Lu, J. Temperature measurement with compositional correction of gas mixture based on laser-induced plasma. *Appl. Opt.* **2020**, *59* (25), 7638−7645.
(36) Dong, M.; Lu, J.; Yao, S.; Zhong, Z.; Li, J.; Li, J.; Lu, W. Experimental study on the characteristics of molecular emission spectroscopy for the analysis of solid materials containing C and N. *Optics express.* **2011**, *19* (18), 17021−17029.
(37) Mousavi, S. J.; Hemati Farsani, M.; Darbani, S. M. R.; Mousaviazar, A.; Soltanolkotabi, M.; Eslami Majd, A. CN and C_2 vibrational spectra analysis in molecular LIBS of organic materials. *Appl. Phys. B: Lasers Opt.* **2016**, *122* (5), 106.
(38) Guizani, C.; Haddad, K.; Limousy, L.; Jeguirim, M. New insights on the structural evolution of biomass char upon pyrolysis as revealed by the Raman spectroscopy and elemental analysis. *Carbon.* **2017**, *119*, 519−521.
(39) Sheng, C. Char structure characterised by Raman spectroscopy and its correlations with combustion reactivity. *Fuel.* **2007**, *86* (15), 2316−2324.
(40) Sommariva, S.; Maffei, T.; Migliavacca, G.; Faravelli, T.; Ranzi, E. A predictive multi-step kinetic model of coal devolatilization. *Fuel.* **2010**, *89* (2), 318−328.

■ NOTE ADDED AFTER ASAP PUBLICATION

This paper was published ASAP on April 9, 2024. The Title of the paper was updated, and the corrected version was reposted on April 10, 2024.

https://doi.org/10.1021/acs.energyfuels.4c00154
Energy Fuels 2024, 38, 7929−7940